REPORT DOCUMENTATION PAGE

Public Reporting burden for this collection of information is estimated to average 1 hour per response, including the time for reviewing instructions, searching existing data sources, gathering and maintaining the data needed, and completing and reviewing the collection of information. Send comment regarding this burden estimates or any other aspect of this collection of information, including suggestions for reducing this burden, to Washington Headquarters Services, Directorate for information Operations and Reports, 1215 Jefferson Davis Highway, Suite 1204, Arlington, VA 22202-4302, and to the Office of Management and Budget, Paperwork Reduction Project (0704-0188,) Washington, DC 20503.

1. AGENCY USE ONLY (Leave Blank)	2. REPORT DATE April 19, 2007	3. REPORT TYPE AND DATES COVERED Final :02/16/2004-02/17-2007

4. TITLE AND SUBTITLE Mathematical Fluid Dynamic Modeling of plasma Stall-Spin Departure Control	5. FUNDING NUMBERS AFOSR Contract FA9550-04-C-0028
6. AUTHOR(S) Norman D. Malmuth, Alexander V. Fedorov and Victor Soloviev	

7. PERFORMING ORGANIZATION NAME(S) AND ADDRESS(ES) Teledyne Scientific LLC, 1049 Camino Dos Rios, Thousand Oaks, California 91360	8. PERFORMING ORGANIZATION REPORT NUMBER SC71234.RFRFTV

9. SPONSORING / MONITORING AGENCY NAME(S) AND ADDRESS(ES) Air Force Office of Scientific Research 875 N. Randolph Street Arlington, VA 22203 Dr Arje Nachman/NE	10. SPONSORING / MONITORING AGENCY REPORT NUMBER

11. SUPPLEMENTARY NOTES
    The views, opinions and/or findings contained in this report are those of the author(s) and should not be construed as an official Department of the Army position, policy or decision, unless so designated by other documentation.

12 a. DISTRIBUTION / AVAILABILITY STATEMENT Approved for public release; distribution unlimited.	12 b. DISTI AFRL-SR-AR-TR-07-0140

13. ABSTRACT

This report summarizes theoretical and CFD studies related to surface discharge to quench stall-slip departure due to asymmetric vortex shedding on aircraft nose tips, augment directional control/authority, agility and develop tailless capability. This approach offers adaptability to rapidly changing flight and mission conditions, constructional simplicity, massless operation, no changes in aerodynamic shape, no influence on aircraft characteristics when the system is not in use and low weight and power penalties, and closed loop feedback control. In the first phase of the effort, lower-order theoretical modeling showed that vortex symmetry breakdown strongly depends on the boundary-layer separation locus. The latter can be effectively controlled by a surface discharge located upstream from the separation line. Using spark discharges of relatively small power (less than 1 kW) it is feasible to shift the separation line toward the windward surface and suppress vortex asymmetry. In the second phase, more comprehensive computational tools were developed to provide data for validation and calibration of our lower-order theoretical models. The Conical Navier-Stokes (CNS) solver was developed and applied to simulate vortex structures over a cone at high angles of attack for laminar and turbulent flows. Numerical solutions satisfactorily predict characteristics of symmetric and asymmetric turbulent flows observed in the subsonic wind-tunnel experiments. The CNS solver was used for modeling of the spark-discharge effect on vortex asymmetry past a sharp cone at high angles of attack. To simulate local heating induced by the discharge, a source term was added to the energy equation. The CNS predictions qualitatively agree with the experimental observations. Namely, the heat source causes early separation and reduces the vortex flow asymmetry. With two symmetric heat sources located on opposite sides of the cone cross-section it is feasible to restore the symmetric flow pattern and eliminate the side force. Numerical studies showed that the side force reveals a hysteretic behavior versus the source intensity. The side force control law may reveal non-monotonic features depending on the angle of attack and heat source intensity. The major gap in plasma flow control technology is the lack of self-consistent theoretical models and robust computational tools providing adequate simulation of heat and momentum sources induced by surface plasma discharges. First steps in solving this problem were made for the surface barrier discharge (SBD). The physical and numerical models developed capture the streamer phase of SBD evolution. This provides a good starting point to address the relaxation phase and treat the whole SBD cycle produced by an alternating applied voltage.

14. SUBJECT TERMS Vortex symmetry breakdown, stall-slip departure control, surface discharge, conical Navier-Stokes method, high angle of attack, side force control, surface barrier discharge	15. NUMBER OF PAGES 36
	16. PRICE CODE

17. SECURITY CLASSIFICATION OR REPORT **UNCLASSIFIED**	18. SECURITY CLASSIFICATION ON THIS PAGE **UNCLASSIFIED**	19. SECURITY CLASSIFICATION OF ABSTRACT **UNCLASSIFIED**	20. LIMITATION OF ABSTRACT UL

NSN 7540-01-280-5500

Standard Form 298 (Rev.2-89)
Prescribed by ANSI Std. 239-18
298-102

Mathematical Fluid Dynamic Modeling of Plasma Stall-Spin Departure Control

Final Report

on AFOSR Contract FA9550-04-C-0028

for the period 02/16/2004 thru 02/15/2007

Prepared by:

Drs. Norman D. Malmuth, Alexander V. Fedorov and Victor Soloviev
Teledyne Scientific Company
Thousand Oaks, CA 91360

April 2007

Executive Summary

This report summarizes effort performed under AFOSR contract FA9550-04-C-0028. It describes theoretical and CFD studies related to surface spark discharge to quench stall-slip departure due to asymmetric vortex shedding on fighter aircraft nose tips, augment directional control/authority, agility and develop tailless capability.

Despite extensive research of symmetric vortex breaking, a major deficiency is limited understanding of the underlying basic physical processes such as vortex flow instabilities near forebody noses as they pertain to bifurcations of the vortex structure. These deficiencies are evident in the scope of previous experimental, theoretical, engineering and CFD studies.

Although empirical fixes such as strakes have been successfully used for asymmetric vortex-induced yaw departure problems on current generation aircraft such as the X-31 and F-18 HARV) research and design of more efficient and robust flow control devices are needed. One of the most promising techniques is a high-frequency discharge on the forebody surface. Compared to previous control devices such as strakes and jets, this approach offers adaptability to rapidly changing flight and mission conditions, constructional simplicity, no plumbing or volume or bleed air penalties, massless operation, no changes in aerodynamic shape; no influence on aircraft characteristics when the system is not in use and low weight and power penalties on typical flight vehicles. Moreover, discharge frequency and power variation allow optimal flow disturbances and closed loop feedback control.

The first phase of this project clearly showed that vortex symmetry breakdown strongly depends on the boundary-layer separation locus. The latter can be effectively controlled by a surface discharge located upstream from the separation line. Using spark discharges of relatively small power (less than 1 kW) it is feasible to shift the separation line toward the windward surface and stabilize symmetric vortex structure. Such power levels can be easily accommodated on aircraft. With our theoretical guidance and under complementary EOARD support, the Institute of Theoretical and Applied Mechanics (ITAM, Novosibirsk) performed a series of wind-tunnel experiments demonstrating the ability to control the vortex asymmetry with the help of spark discharges. ITAM validated the theory and even provided a working spark discharge arrangement that avoids symmetry breaking on a conical nose tip typical of actual aircraft shapes.

In the second phase (2004-2006), the effort has been focused on development of more comprehensive computational tools, which could provide data for validation and calibration of our lower-order theoretical models. By examining available numerical methods, which have been used for modeling of the vortex flow over a cone at high angles of attack, we concluded that methods based on the Conical Navier-Stokes (CNS) equations fit our needs. The CNS equations are an approximate form of the 3-D Navier-Stokes equation. They differ from the full equations by the assumption of constant properties in the radial direction. Nevertheless, the conical solutions reproduce symmetric and asymmetric vortex configurations, which are similar to those observed in experiments. As contrasted to our earlier lower-order models, in which the separation points were fixed à priori, the CNS method captures the interaction between viscous boundary layer and inviscid outer flow and predicts separation lines.

In 2004, the CNS solver has been developed and applied to modeling of vortex structures over a cone at high angles of attack. The first series of calculations conducted for laminar flow showed that the CNS solver reproduces symmetric and asymmetric vortex fields and can be used for estimation of the critical angle of attack at which the vortex symmetry breaks down. However, the wind-tunnel experiments of ITAM and the majority of full-scale flight applications correspond to turbulent flow. This motivated us to focus our 2005 effort on CNS modeling of vortex structures for turbulent boundary layers.

In 2005, the CNS solver has been extended to turbulent boundary layers for modeling of the vortex symmetry breaking. Comparative analysis of different two-parameter turbulent models showed that these standard models should be modified in order to simulate three-dimensional turbulent flows with significant adverse pressure gradients, separated shear layers and strong vortices outside the boundary layer. To achieve good agreement with experimental results it is necessary to reduce, or even eliminate the turbulent eddy-viscosity in the leeward-side vortices. This was accomplished using a Galilean-invariant leeward vortex filter. The modified k-ε EASM model was incorporated into our CSN solver. Parametric calculations showed that numerical solutions obtained with this model satisfactorily predict characteristics of symmetric and asymmetric turbulent flows observed in the subsonic wind-tunnel experiments. The k-ε EASM model was recommended for further studies of the surface plasma discharge effect on the vortex structure.

In 2006, we used the CNS solver for modeling of the forebody vortex symmetry plasma control. In particular, we considered spark-discharge forcing of turbulent boundary-layer separation and vortex asymmetry on a sharp cone at high angles of attack. To simulate local heating induced by the spark discharge, a source term was added to the energy equation in a simple analytical form. A first series of calculations for one energy source located at the cone cross-sectional equator showed that CNS predictions are qualitatively similar to our experimental observations. Namely, the heat source (located on the side with farther vortex) causes early separation and reduces the vortex flow asymmetry. Calculations showed that with two symmetric heat sources located on opposite sides of the cone cross-section it is feasible to restore the symmetric flow pattern and eliminate the side force. For one source, there is a critical value of the source intensity at which the flow asymmetry and corresponding side force change sign. The side force reveals a hysteretic behavior versus the source intensity. These examples indicate that the side force control law may reveal non-monotonic features depending on the relative angle of attack and heat source intensity. We also considered the convergence history of the conical solution with the energy source activated during a finite time period. It was shown that the length of transition from a nearly symmetric to an asymmetric state might be of the order of the actual body length. Accordingly, it is important to perform adequate modeling of the transition process. In this connection, part of our future effort will be focused on theoretical and 3-D Navier-Stokes CFD studies of the downstream evolution of an originally symmetric vortex flow to an asymmetric state.

A major gap in plasma flow control technology is the lack of self-consistent theoretical models and robust computational tools providing adequate simulation of heat and momentum sources induced by surface plasma discharges. To bridge this gap, we plan to conduct comprehensive theoretical and computational studies of the plasma surface discharge physics. First steps in solving this problem were made under EOARD sponsorship (ISTC Project 2235). Preliminary calculations indicated that our physical and numerical models capture the streamer phase of

surface barrier discharge (SBD) evolution. This provides a good starting point to address the relaxation phase and treat the whole SBD cycle produced by an alternating applied voltage.

With our refined theoretical and CFD tools, we are well positioned to investigate effects of external forcing produced by surface plasma dischargers and address the problem of plasma stall spin departure control as well as aerodynamic augmentation of high altitude, long endurance aircraft. We plan to target plasma control of the interaction of separation and transition as well as vortex breakdown in connection with this application and others. An EOARD-ISTC experimental complement to this study is being performed by our ITAM team in connection with schemes to control the flow over high-speed wings.

Table of Contents

List of Figures

1. Background

High angle of attack maneuvering capability is critical for mission survivability of modern fighter aircraft [1]. A key element is freedom from stall and slip departure that can occur because of asymmetric forebody vortex formation. A pointed axisymmetric body at sufficiently large angles of attack experiences a side force associated with formation of asymmetric vortex structures (Figure 1). Continuing experience with current inventory aircraft such as the Northrop F-5, F-18 and the Rockwell X-31 shows that the asymmetric vortex phenomenon can produce forces and moments that are large and evolve rapidly. Both factors may result in a loss of control due to the reaction limitations of the pilot and lack of control authority. Conventional solutions of this problem are strakes, slot blowing and engine thrust-vectoring.
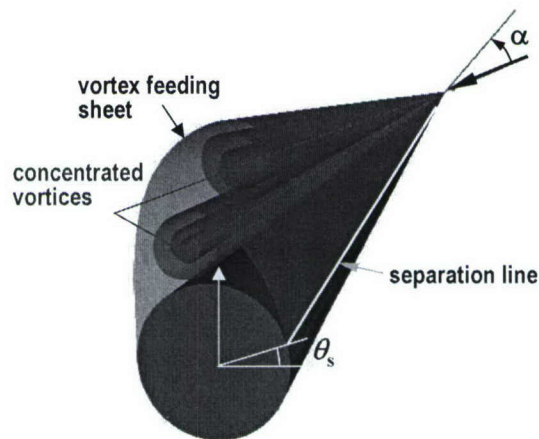
Figure 1 Vortical flow over a cone at high angle of attack.
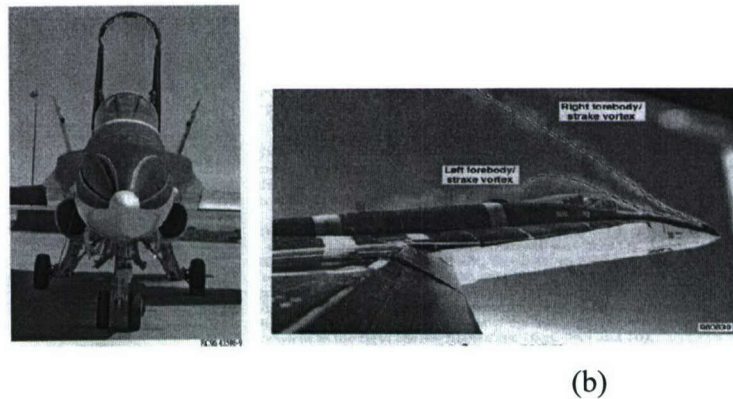
Figure 2 Actuated strakes (a) and forebody vortex formation (b) on F-18 HARV (from Banks et al. 1994).

Fixed geometry strakes as well as chines could be a point design that might not resolve the stall-spin tendency over the entire flight envelope. Variable and actuated strakes (Figure 2) might be a more global flight envelope solution. However, they may compromise flying qualities, aerodynamic performance as well as stability and control. They also introduce mechanical complexity and weight issues. Blowing and thrust vectoring may require too much engine bleed air to be effective. MEMS is another possibility, although special micro-fabrication and basic understanding and continuing research is needed to account for the complex issues of this flow in the control laws.

Feasibility studies of the first phase of this project (see Section 2) show that plasma surface discharges can be effectively used to control the forebody vortex structure.[†] Symmetrical tripping of the boundary layer by a simple plasma discharge device may be advantageous compared to the aforementioned schemes due to its simplicity, potential effectiveness and attractiveness for a close-loop feedback system that might include co- and counter-phasing. A schematic of a plasma control system is shown in Figure 3. A potential high impact flip-side opportunity that may have some low-hanging fruit is to use the stall-slip departure tendency for *yaw control* and *tailless* capability. This could be one possible outcome of the plasma solution.
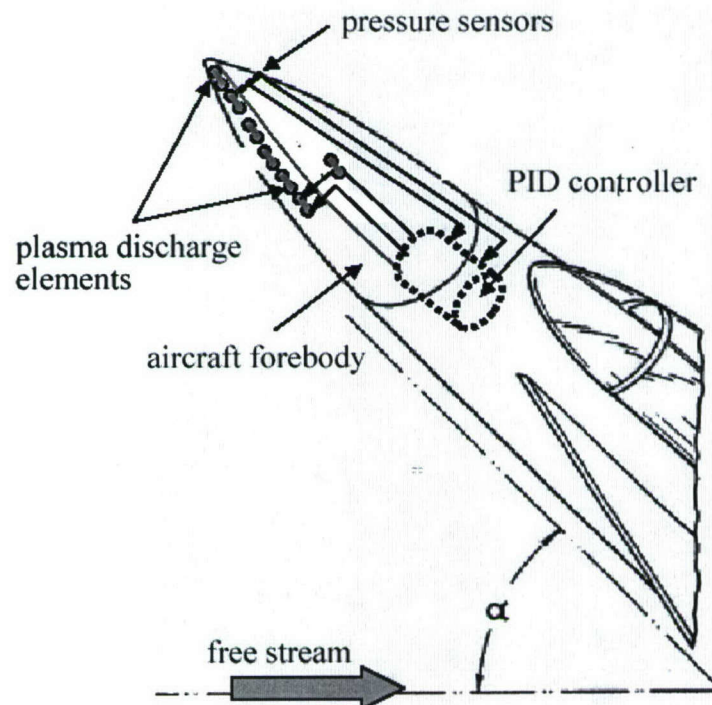
Figure 3 Schematic of discharge system for stall-spin departure control.[†]

Although the problem of forebody vortex symmetry breaking has received much attention [2], important needs must be met before stable and reliable high-angle-of-attack flight can be

---

[†] Malmuth, N., Fedorov, A., Soloviev, V., Maslov, A., Zharov, V., Shalaev, I., Surface Plasma Discharge For Controlling Forebody Vortex Asymmetry, US Pat. No. 6,796,532 (09/28/2004)

achieved. One of the difficulties is accurate simulation of the unsteady aerodynamic forces and moments due to the unsymmetrical flow pattern. Because the underlying physical mechanisms are not well understood, development of control devices is relegated to trial and error. The related lack of simulation capability complicates implementing robust fixes on operational aircraft.

The practical importance of the asymmetric vortex phenomenon has prompted much experimental [3]–[14] and theoretical [15]–[20] research. Asymmetrical flow fields arise near the fuselage nose. Downstream from this region, the body shape slightly affects the vortex structure [3]–[5], [7]–[9], [12], [13], [17]–[19]. This feature suggests control of the vortex asymmetry by perturbations close to the nose [3]–[5], [17]–[19] and leads to research on forebodies of simple shape, such as cone and ogive cylinders [3], [4], since most noses can be approximated by such shapes.

Occurrence of asymmetry is related to absolute rather than convective and nonlinear rather linear instabilities of the symmetrical flow field [14], [15]. This leads to strong dependence of the flow pattern on small disturbances, such as vibration of the nose and its roughness [3], [4] and [12], distortion of the nose shape [3], [4], [17]–[19], freestream disturbances [3], [7], [8]. The physics of this instability is not yet understood. The lack of reliable theoretical models has precluded identifying a clear criterion for the origin of instability and development of asymmetry.

The vortex symmetry breaking strongly depends on boundary-layer separation, which might be very sensitive to small-scale, freestream disturbances and high frequencies (e.g., noise, turbulence, body vibrations, roughness). Criteria for experimental simulation of the boundary-layer flow and its separation must account for dependence on Reynolds number (viscous effects), and varying level of freestream disturbances (which may be minimized in quiet wind tunnels). Experimental designs should also include roughness and waviness of the model. These criteria are not accounted for in routine aerodynamic experiments. Furthermore, the problem of aerodynamic force simulation is complicated by an ambiguous role of external disturbances that can affect the global flow field. In this connection, data obtained in different wind tunnels weakly correlate with each other [3], [21]. Also, they are not easily extrapolated to flight conditions.

This research, and complementary experimental effort of the Institute of Theoretical Mechanics (ITAM) in Novosibirsk Russia, sponsored by the ISTC/EOARD Project-2235 project, is filling these gaps. Our theoretical studies are based on a combined numerical and asymptotic approach. The major thrust is related to surface discharge plasmas and other plasma devices to quench stall-slip departure due to asymmetric vortex shedding on fighter aircraft nose tips, augment directional control/authority, agility and develop tailless capability.

2. Major accomplishments

An overview of the project effort is shown in Figure 4. The effort includes the two major components:

1. Plasma discharge modeling
2. Fluid dynamics modeling
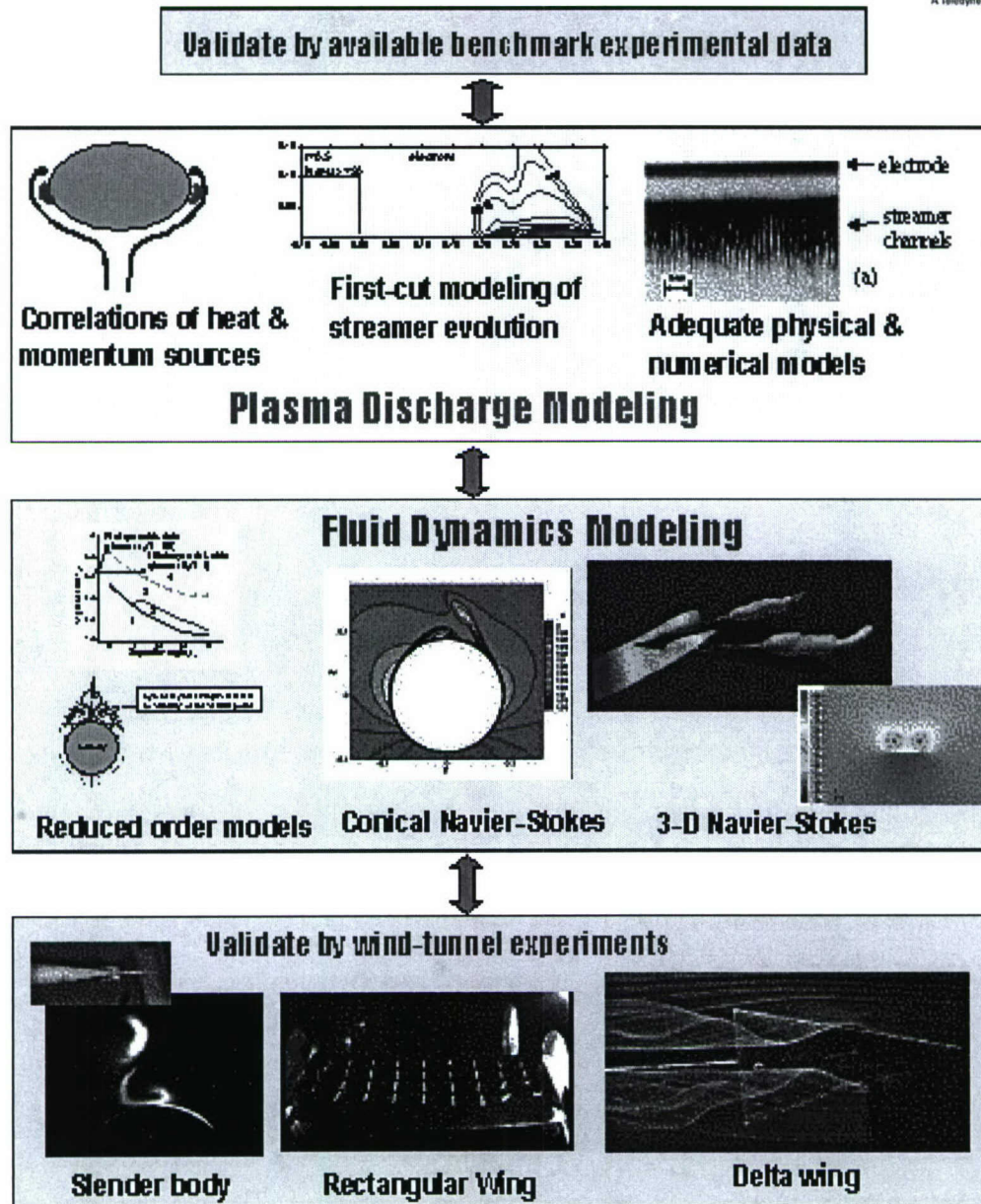
Figure 4 Project overview with major components.

The first component is focused on development of self-consistent theoretical models and robust computational tools providing adequate from-first principles-simulation of heat and momentum sources induced by surface discharges. The second component deals with development of theoretical (lower-order) and computational models of fluid dynamics relevant to plasma flow control applications. These two components are strongly coupled and aimed at the development of a combined theoretical and computational toolbox for plasma flow control applications. The theoretical and computational effort is anchored by the experimental effort conducted under a separate complementary program at the Institute of Theoretical and Applied Mechanics (Novosibirsk, Russia) to provide a cohesive and cost-effective attack on the plasma actuator problem.

Currently we study stall-slip departure control associated with asymmetric vortex shedding on aircraft nose tips. Natural continuation of this effort will be the vortex flow control on delta wings. This fluid dynamics problem perfectly fit to plasma flow control application because delicate local forcing of separated boundary layer leads to global changes of the vortex flow and its asymmetry that, in turn, strongly affects side forces. This opens up an opportunity to eliminate symmetry breaking, preserve lift, augment lateral control authority, delay vortex breakdown and augment tailless capability of various aircraft.

2.1 Accomplishments of the 2001-2003 effort

In FY-2001-2003, we conceptualized a theoretical model of the vortex dynamics and estimated feasibility of the vortex structure control using a surface discharge on a sharp slender cone at angles of attack [P1]. We started with theoretical modeling of the flow asymmetry occurrence on a sharp cone at high angle of attack. From slender body theory and point vortex modeling of the inviscid flow we found that the symmetry breaking is associated with nonlinear instability of the saddle point occurring over the body surface as schematically shown in Figure 5.
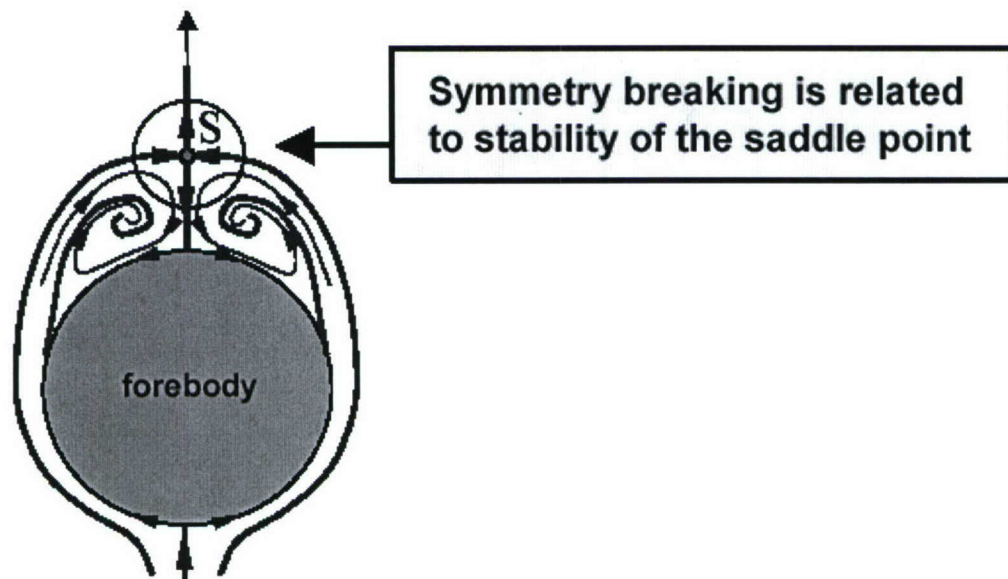
Figure 5 Saddle point over the body surface.

It was shown that the saddle point trajectories are governed by the Ginsburg-Landau (GL) equation. Analysis of this equation indicated that the saddle point is nonlinearly unstable under supercritical conditions. If a periodic forcing of the saddle point is larger than a certain critical level (red dashed line in Figure 6), then the saddle-point oscillations quickly increase downstream and attain a spike-like shape. The amplitude of these spikes tends to infinity at a finite distance from the tripping element. This trend indicates that the symmetric flow pattern breaks down and evolves to an asymmetric state at finite distance from the tripping element.
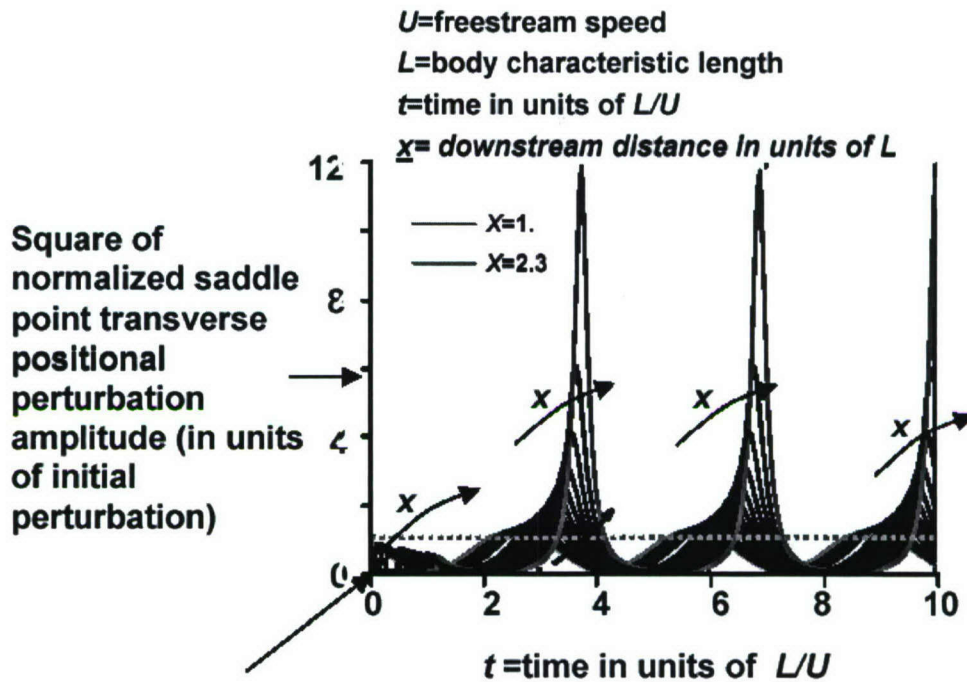
Figure 6 Saddle-point instability predicted by Ginsburg-Landau equation.

Using nonlinear solutions of the GL equation (with coefficients related to our problem), we established the criterion of symmetry breaking (red lines in Figure 7) in terms of the boundary-layer separation angle θ_s (this angle is shown in Figure 1-1) and the normalized angle of attack $\alpha \equiv \alpha^* / \delta$, where δ is cone half angle. An additional parameter, λ, specifies the cross-sectional thickness of the body. Parametric calculations were performed for slender elliptic cones with λ varying from 0.01 (thin delta wing) to 1 (circular cone) for a wide range of separation angles and normalized angles of attack $\alpha = 1 - 10$. The criterion of saddle-point stability correlates well with the experimental data [14] for round (circles) and elliptic (rhombus) cones. As $\delta \to 0$, the experimental data for circular cones converge to the theoretical curve of saddle-point occurrence estimated from the first-order approximation of slender body theory. For elliptic cones, the experimental points practically lie on the theoretical curve of saddle-point occurrence although the expansion parameter is not very small. The discrepancy between data and calculations for thin delta wings is more appreciable since vortex breakdown and the boundary layer state (laminar or turbulent) influence the asymmetry in this case. When this does not occur, the discrepancy between theory and experiments is of the same order as that for a right circular cone of the same apex angle. Details of this comparison are given in [P4].

As shown in Figure 8, the breakdown of symmetric vortex structure strongly depends on the separation locus that can be effectively controlled by a surface discharge located azimuthally upstream from the separation line. Using discharges of relatively small power (less than 1 kW) *that are easily deployed on modern flight vehicles*, it is feasible to shift the separation line toward the windward surface and stabilize the symmetric vortex structure.
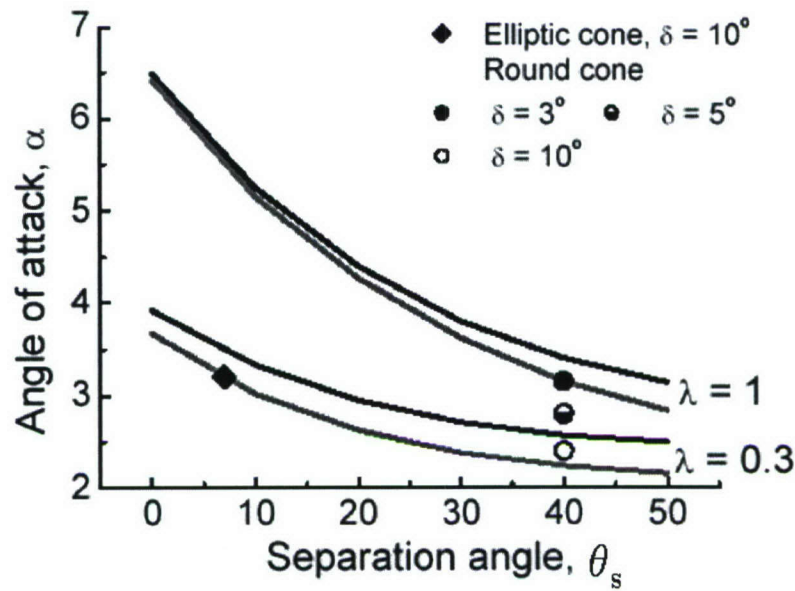
Figure 7 The theoretical criterion of vortex symmetry breaking (red lines) agrees well with the experimental data [14] (symbols); circles – round cones of half angles $\delta = 3°, 5°, 10°$; rhombus – elliptic cone of the axes ratio $\lambda = 0.3$.
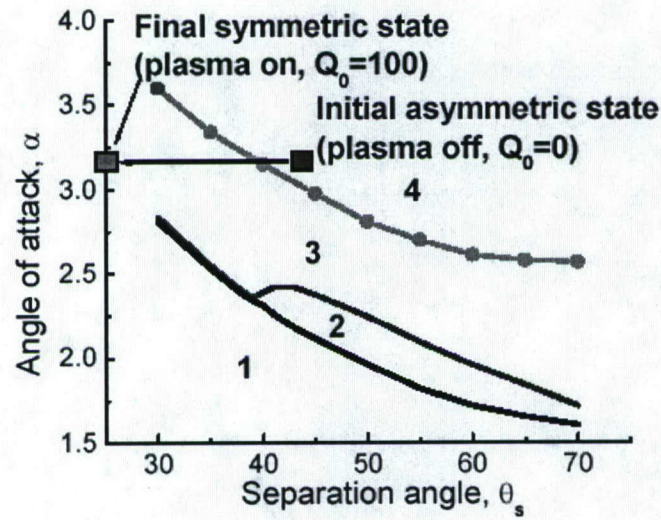
Figure 8 Movement of blue point to red point from symmetry breaking zone to symmetric vortex zone with plasma Joule heating. Region 1 - no vortices; Region 2 - only one solution with two symmetric vortices; Regions 3 and 4 – there are symmetric and asymmetric solutions. In Region 3 symmetric solution is stable; in Region 4 symmetric solution is unstable.

2.2 Accomplishments of the 2004-2006 effort

In our previous studies [P1,P4] the inviscid point vortex-pair model has been used to simulate the vortex structure over a slender body at incidence. However, we found that this model is not adequate to account for the coupling of the inviscid flow with the viscous boundary layer, since it is ineffective in iterative calculations of the separation loci and the production of feeding sheets that create the large-scale vortex dynamics and fractal structures associated with high angles of attack. Moreover, the boundary-layer solution becomes singular approaching the separation region complicating the prediction of separation lines and simulation of the coupling between boundary-layer separation and global large-scale vortical dynamics, which traditionally and with some success has been simulated as an inviscid vortex flow. This inadequacy motivated us to develop a more sophisticated computational tool, which captures the viscous-inviscid interaction and at the same time is not computationally intense. The latter requirement is important for quick assessments of vortex flow control by surface discharges of various shapes and intensity.

By examining available numerical methods, that have been used for modeling of vortex flows over cones at high angle of attack, we concluded that methods based on the Conical Navier-Stokes (CNS) equations [22] fit our needs. The conical solutions reproduce symmetric and asymmetric vortex structures, which are similar to those observed in experiments. The major advantage of the CNS method is that it requires computations in only two dimensions, thereby considerably reducing computation cost. Although the flow is not purely conical when viscous effects are taken into account, conical similarity is a reasonable first approximation since the vortex feeding sheets still appear to emanate along the cone generators. An important concern in this simplification is the adequacy of the conical similarity. This is an area of future research. Nevertheless, preliminary indications suggest that it may be adequate to describe the flow field in certain important regimes of interest. Heuristically we expect that conical similarity may be valid for boundary layers that are thin.

The CNS method has been accomplished using the PSENS (Parallel Structured Euler, Navier-Stokes) solver [23] modified by Dr. Zakharov. This code solves Navier-Stokes equations for 3-D compressible flows using the MUSCL upwinding procedure with Roe's flux difference splitting for the mean flow equations coupled to the turbulence model equations. Viscous terms are discretized using the second-order central differences in either the thin-layer or full Navier-Stokes form. The temporal integration is accomplished with an implicit, diagonalized, approximate factorization scheme. In our approach, the 3-D Navier-Stokes equations are written in spherical coordinates. These equations are solved in a thin region $(R_0, R_0 + \Delta R)$, which contains four grid points along the axial coordinate (see Figure 9). The boundary conditions on the upstream ($R = R_0$) and downstream ($R = R_0 + \Delta R$) planes with local conical invariance is formulated as

$$\left(u, v, w, \rho, p\right)_{R=R_0} = \left(u, v, w, \rho, p\right)_{R=R_0+\Delta R}. \tag{1}$$

No-slip conditions are imposed on the cone surface of radius r_{min}, which is the inner boundary of computational domain. The non-reflecting boundary condition resulted from 1-D Riemann invariants are formulated on the outer boundary of radius r_{max}.
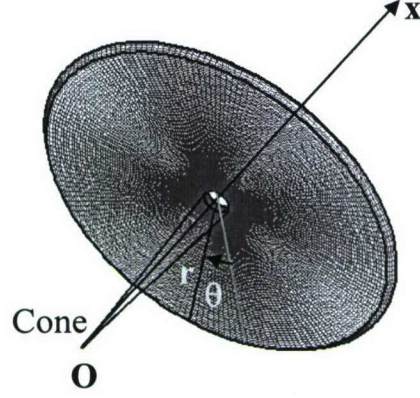
Figure 9 Coordinate system and computational domain.

An O-grid is generated on the upstream plane $R = R_0$. This grid is homogeneous in the azimuthal direction (the number of grid points in this direction $m = 180$) and is clustered near the cone surface as

$$r(j) = 1 + (r_{max} - 1) \left(1 - s + \frac{2s}{1 + \left[\frac{s+1}{s-1} \right]^{\frac{n-j}{n-1}}} \right), \quad j = 1, n, \quad (2)$$

where $n = 101$ is number of the grid points in the radial direction, $s = 1.025$ is compression factor, the outer boundary radius is $r_{max} = 15 r_{min}$. This grid is continued to the downstream plane along spherical radii. The grid clustering was also performed in the azimuth direction (from $\Delta \varphi \approx 3°$ on the windward to $\Delta \varphi \approx 1°$ on the leeward side) using the relation

$$\varphi(i) = \varphi(i-1) - \frac{\pi}{180} \left(2.1 - \sin(\varphi(i-1)) \right), \quad i = 1, n_\varphi / 2, \quad \varphi(0) = \frac{3}{2} \pi, \quad (3)$$

where n_φ is number of the grid points in the azimuth direction.

The following models of turbulence have been investigated: k-epsilon EASM [24], k-omega ESAM [24], and various modifications of k-epsilon model presented in Refs. [25-27]. Parametric calculations showed that the extension of standard turbulence models, which have been developed for attached boundary layers and wake flows, to highly three-dimensional flows with significant adverse pressure gradients, separated shear layers and strong vortices outside the

boundary layer is not straightforward. The major difficulty is associated with modeling of the turbulent eddy viscosity in regions of high vorticity.

In order to achieve good agreement with experimental results it is necessary to reduce, or even eliminate the turbulent eddy-viscosity in the leeward-side vortices. This was done using a Galilean-invariant leeward vortex filter

$$H_v = \tanh\left(\frac{|I_2 v^2|}{H_{\max}}\right), \tag{4}$$

where v is local cell volume; $H_{\max}$ is constant determined empirically;

$I_2 = \begin{vmatrix} U_x & V_x \\ U_y & V_y \end{vmatrix} + \begin{vmatrix} V_y & W_y \\ V_z & W_z \end{vmatrix} + \begin{vmatrix} U_x & W_x \\ U_z & W_z \end{vmatrix}$ - is Galilean-invariant reliably responds to vorticity outside

the boundary layer. The invariant I_2 does not distinguish between a free vortex and vorticity within the boundary layer. This is remedied with scaling of I_2 by the local cell volume v, which is also invariant. Small cells within the boundary layer receive much less of a contribution than larger cells in the vortex region.

Equation (4) is applied to a particular turbulence model by modifying the turbulence production term. For example, the eddy-viscosity production term of the Spalart-Allmaras model is

$$P = c_{b1} v_t |\omega|, \tag{5}$$

where c_{b1} is a scalar coefficient, v_t is turbulent eddy-viscosity, and ω is vorticity. This production term was modified as

$$P' = P(1 - H_v), \tag{6}$$

The filtering (6) reverts to the original formulation within the boundary layer ($H_v \to 0$), and removes the production of eddy-viscosity in the leeward-side vortices ($H_v \to 1$).

With this modification of the vortex filter we carried out series of computations and showed that the k-ε EASM model with $H_{\max} = 5 \times 10^{-12}$ provides the best fit of separation angles to experimental values. For the k-ε model, this is achieved with $H_{\max} = 2 \times 10^{-12}$.
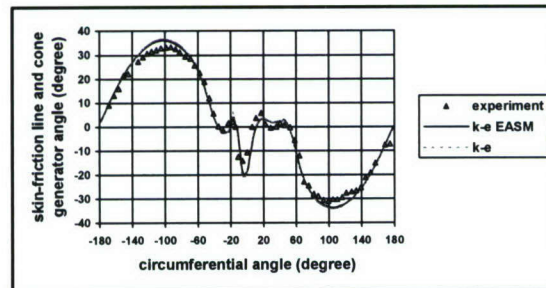
Figure 10 Angle between the skin friction lines and the cone generator as a function of the circumferential angle φ; Mach number $M_\infty = 0.6$, Reynolds number $\mathrm{Re}_x = 9.8 \times 10^6$; asymmetrical flow at $\alpha = 3$.

Figure 10 shows the angle ψ_f between the skin-friction lines and the cone generator as a function of the circumferential angle φ. The numerical predictions of this distribution are close to each other (compare the black solid line with the red dashed line) and agree well with the experimental data [28] (symbols) corresponding to $\alpha = 3$.

It was shown that the k-ε EASM model [24], with the vortex filter (4), is appropriate for further CSN modeling of the vortical flow. The CNS solver reproduces symmetric and asymmetric vortex fields (Figure 11), allows for estimations of the critical angle of attack at which the vortex symmetry breaks down (Figure 12), and predicts the side force due to the vortex symmetry breaking (Figure 14). Details of the CNS modeling and comparisons with experimental data are given in [P10].

This study provides a significant improvement over previous symmetry breaking models in which the separation angles and origins of the feeding sheets were assumed. Importantly, the CNS solver is a computationally non-intensive tool, which is convenient for parametric calculations of vortex symmetry breaking and its control and system studies, particularly conceptual design. These results provided a launching pad to continue the CNS modeling of the vortex symmetry breaking and its control.

a)   b)
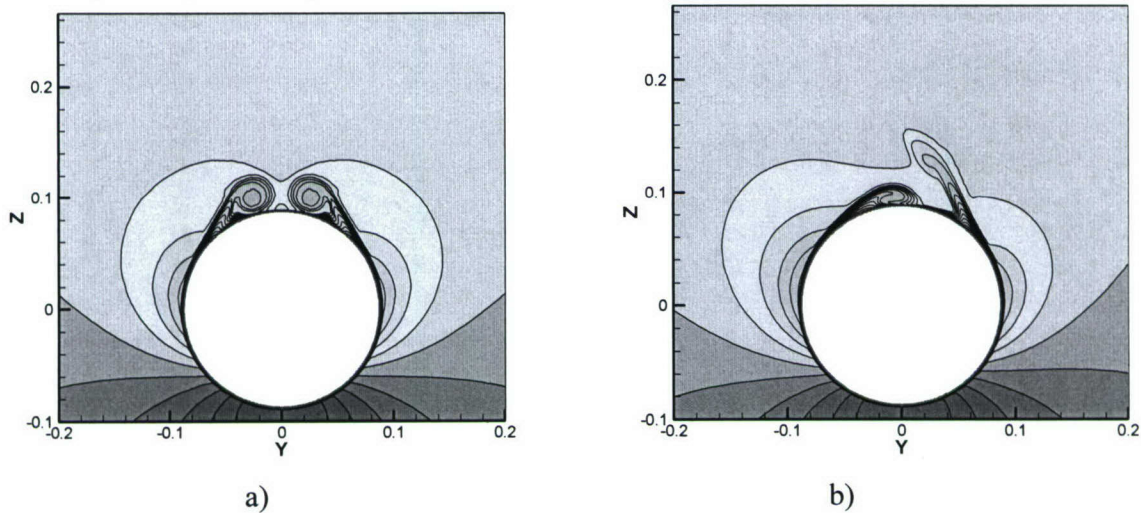
Figure 11 Density field for the intermediate symmetric (a) and final asymmetric (b) solution, $\alpha = 2.5$, $\mathrm{Re}_x = 9.8 \times 10^6$ and $M = 0.6$.
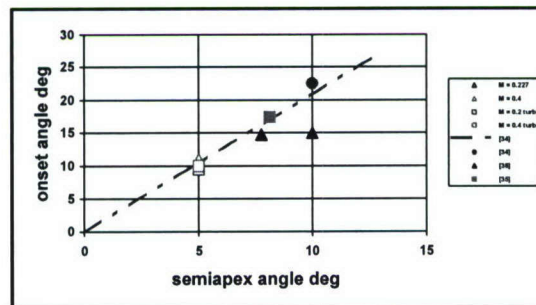
Figure 12 Critical angles of attack versus the cone semi-apex angle, red symbols – CNS prediction, other symbols and blue line - experiments.
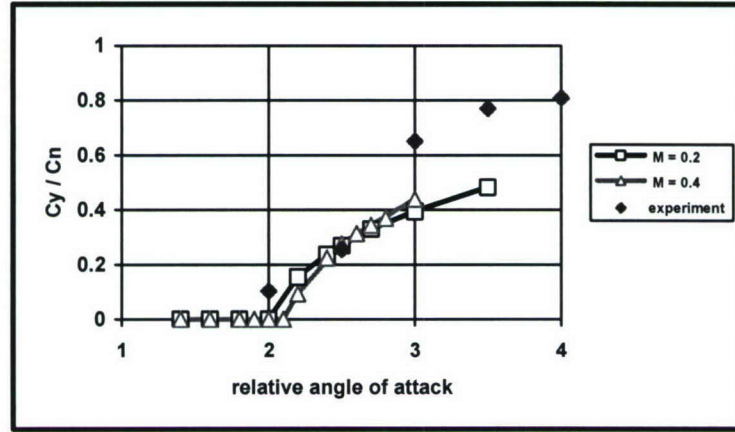
Figure 13 Side-to-normal force ratio as a function of the relative angle of attack α for laminar flow, black line with squares – CNS prediction at Mach=0.2, red line with triangles – CNS prediction at Mach=0.4, blue diamonds – experiment.

In 2006, we used the aforementioned CNS solver for modeling of forebody vortex symmetry plasma control [P12]. In particular, we considered spark-discharge forcing of turbulent boundary-layer separation and vortex asymmetry on a sharp cone at high angles of attack.

To simulate local heating induced by a surface spark discharge we added a source term to the energy equation

$$q = \frac{q^* L^*}{\rho_\infty^* a_\infty^{*3}},\qquad(7)$$

where q^* – power per unit volume, $[q^*]$=[W/m3]; L^* – cone length in x-direction; ρ_∞^* – freestream density, a_∞^* – freestream speed of sound; asterisks denote dimensional quantities. The spatial distribution of heat sources is given by the function $q(r,\varphi)$ that is expressed in the analytical form suggested in Ref. [P1]

$$q(r,\varphi) = q_0 r^2 \exp\left[-\frac{\left[r - r_c(\varphi)\right]^2}{\sigma^2}\right],\qquad(8)$$

where q_0 – heat source intensity, $r_c(\varphi)$ – central line of the discharge arc, σ – scale of the source width, $r = \sqrt{y^2 + z^2} - r_{cone}$ – radial distance from the cone surface. The central line is approximated by the parabolic function

$$r_c = 2r_0 \sqrt{\left|(\varphi - \varphi_1)(\varphi_2 - \varphi)\right|},\qquad(9)$$

where r_0 – maximum distance from the cone surface to the center line, φ_1 and φ_2 – angular locations of the electrodes. The distribution (2) mimics the shape of surface spark discharges

utilized in the experiment [P5]. The dimensionless total power deposited by the source per unit length is

$$Q = \frac{Q^*}{\rho_\infty^* a_\infty^{*3} L^*} = \iint\limits_{(y,z)} q(y,z)\, dydz, \tag{10}$$

where integration is performed over the cross-sectional plane (y,z) of the computational domain.

Preliminary numerical calculations were carried out for a circular cone of half angle $\delta = 5°$, freestream Mach number $M_\infty = 0.6$ and Reynolds number $\mathrm{Re}_L = 9.8 \times 10^6$. The normalized angle of attack is $\alpha \equiv \alpha^* / \delta = 2.5$. Flow turbulence was simulated using the k - ε EASM model with vortex filtering, details of which are discussed in Ref. [P10]. The source spatial parameters are $\sigma = 2 \times 10^{-3}$, $r_0 = 10^{-3}$. The discharge centerline angle, $\varphi_0 = 0.5(\varphi_1 + \varphi_2) = 90°$, corresponds to the cone cross-section equator, the angles of electrodes are $\varphi_1 = \varphi_0 - 5°$ and $\varphi_2 = \varphi_0 + 5°$. For these parameters the discharge energy is deposited predominately in the upper portion of the boundary layer. Figure 2-11 shows the flow energy field corresponding to asymmetric solution without heat source. In this baseline case, the right vortex is located higher than the left vortex. With the heat source ($q_0 = 10^7$) located at the equator on the left side, the solution has lower asymmetry compared with the baseline case (compare flow fields in Figure 14 and Figure 15a). For the source of higher intensity, $q_0 = 1.2 \times 10^7$ (Figure 15,b), the solution predicts the flow with asymmetry being opposite to the baseline case; i.e., the right vortex is lower than the left one. These numerical examples show that the heat source effect predicted by CNS modeling is qualitatively similar to that observed in the experiments [P5].
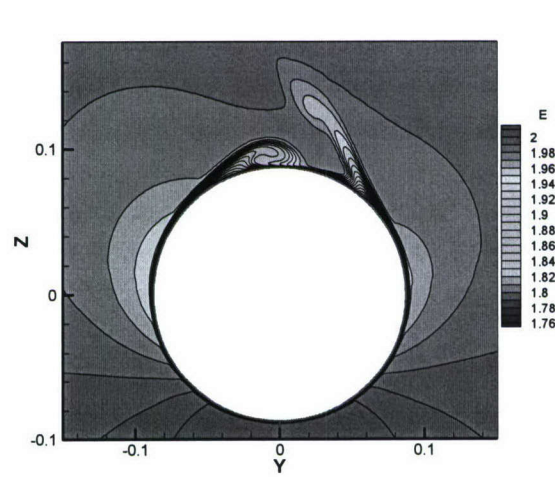
Figure 14 Flow energy field of asymmetric solution without heat sources, angle of attack $\alpha = 2.5$.

(a)

(b)
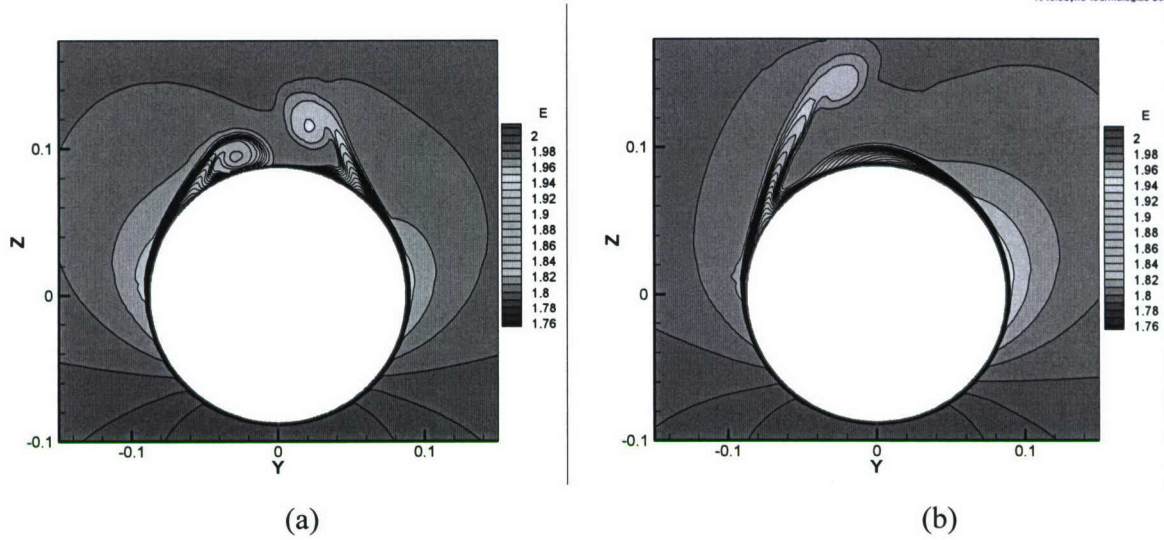
Figure 15 Flow energy field of asymmetric solution with the heat source of $q_0 = 10^7$ (a) and $q_0 = 1.2 \times 10^7$ (b) on the left side, angle of attack $\alpha = 2.5$.

Similar calculations have been performed for two symmetric heat sources of intensity $q_0 = 2 \times 10^7$. For $\alpha = 2.5$, the symmetric heat sources make the originally asymmetric flow pattern become purely symmetric (see Figure 16). This is again consistent with the experimental observations [P5].

(a)

(b)
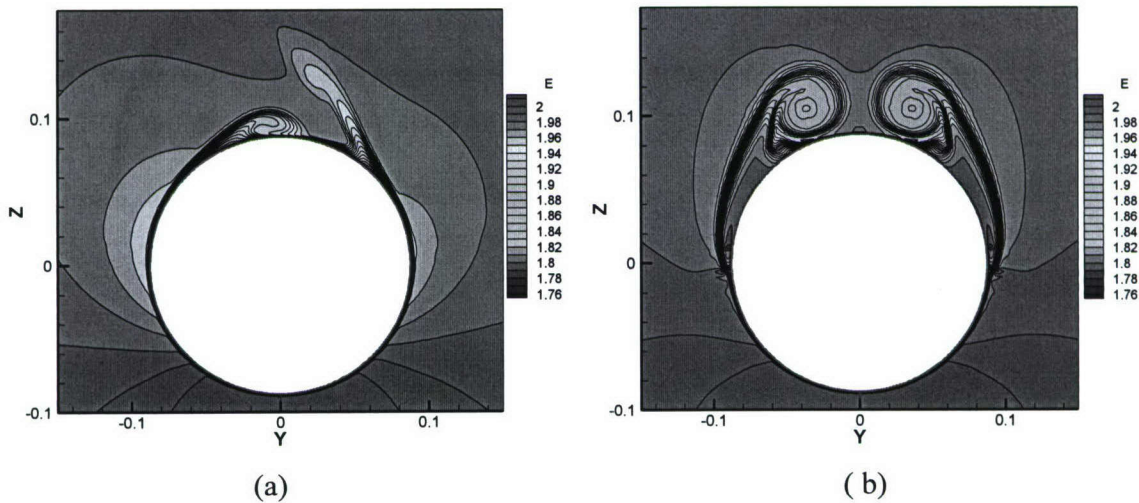
Figure 16 Flow energy patterns: (a) – natural asymmetric flow without heat sources, (b) – symmetric flow with the heat sources on; $\alpha = 2.5$, $M_\infty = 0.6$, $\text{Re}_L = 9.8 \times 10^6$, $q_0 = 2 \times 10^7$.

Figure 17(a) and (b) show the flow energy patterns for the unforced vortex structure and for the flow with the heat sources. Despite symmetric forcing the flow pattern remains asymmetric. Figure 18 shows the side force as a function of the iteration number for the relative angle of attack $\alpha = 2.5$ (a) and $\alpha = 3$ (b). These plots mimic the side force history after activation of the

14

heat sources. Initially, the sources are off and the side force is a negative constant. After switching the heat sources on, the solution converges to a new steady state. The convergence processes are substantially different:

- For $\alpha = 2.5$, the side force monotonically tends to zero; i.e., the solution evolves to a symmetric state.

- For $\alpha = 3$, the side force modulus quickly decreases and then oscillates near a constant level that is presumably associated with a pseudo stable state. After few oscillation periods, the solution monotonically departs from this state and ultimately converges to another state corresponding to a larger side force. Surprisingly, the symmetric forcing leads to an increased side force.

The foregoing examples indicate that the side force control law may have non-monotonic features depending on the relative angle of attack and the heat source intensity. These features need further detailed studies.

(a)   (b)
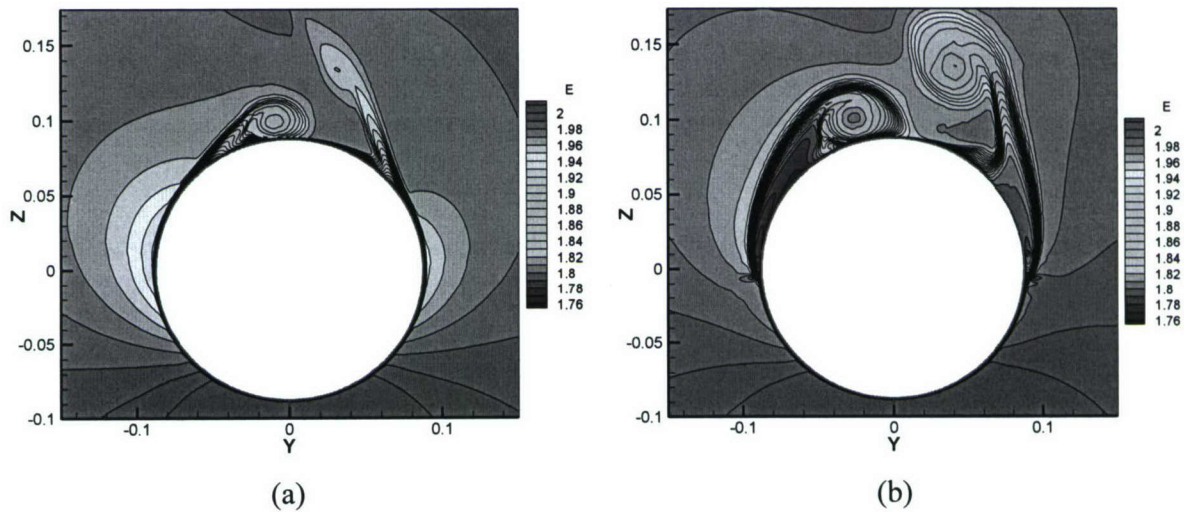
Figure 17 Flow energy patterns: (a) – natural asymmetric flow with the heat sources off, (b) – symmetric flow pattern with the heat sources on; $\alpha = 3$, $M_\infty = 0.6$, $Re_L = 9.8 \times 10^6$, $q_0 = 2 \times 10^7$.

a)   b)
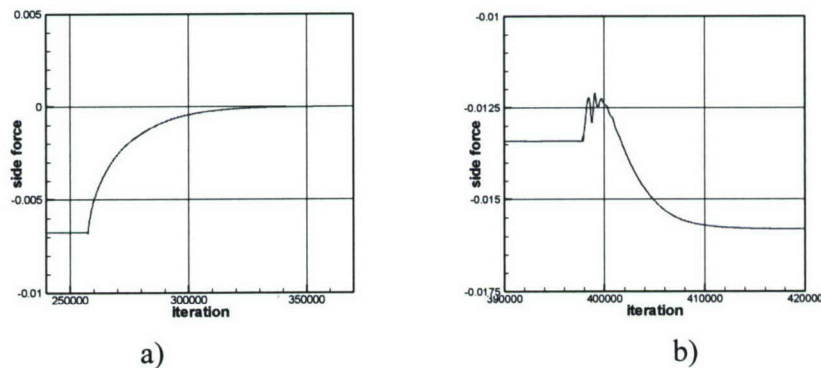
Figure 18 Side force as a function of the iteration number, a) $\alpha = 2.5$, b) $\alpha = 3$; $q_0 = 2 \times 10^7$.

We also investigated effects of the energy source intensity on the vortex asymmetry. Calculations, which were performed for two symmetric heat sources located on opposite sides of the cone cross-section, showed (see Figure 19):

- For a relative angle of attack $\alpha = 2.5$, the heat sources shift the separation lines toward the cross-section equator and make the originally asymmetric flow pattern become purely symmetric. This occurs for the source intensity $q_0 > 14 \times 10^6$.

- For a relative angle of attack $\alpha = 3$, the flow pattern remains asymmetric despite the symmetric forcing up to a source intensity $q_0 = 25 \times 10^6$. During the convergence process, the side force modulus quickly decreases and then oscillates near a constant level that is presumably associated with a pseudo stable state. After few oscillation periods, the solution monotonically departs from this state and ultimately converges to another state corresponding to a larger side force.
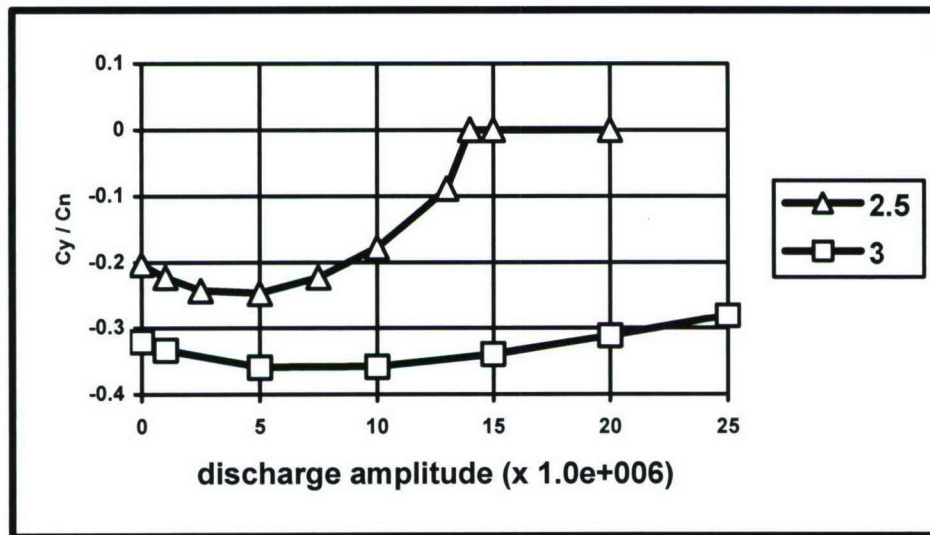
Figure 19 Normalized side force coefficient as a function of nondimensional source intensity q_0 for two symmetric energy sources; line with triangles – $\alpha = 2.5$, line with squares – $\alpha = 3$.

For one source (located on the side where the vortex is closer to the cone surface), there is a critical value of the source intensity at which the flow asymmetry and corresponding side force change sign (see Figure 20). As q_0 increases from zero to this critical value, the side force decreases but does not vanish. At the critical source intensity, the side force jumps to a level that is higher than the original level corresponding to $q_0 = 0$. With further increasing of q_0 the side force slowly increases. Moreover, the side force reveals a hysteretic behavior versus the source intensity. These examples indicate that the side force control law may reveal non-monotonic features depending on the relative angle of attack and the heat source intensity.
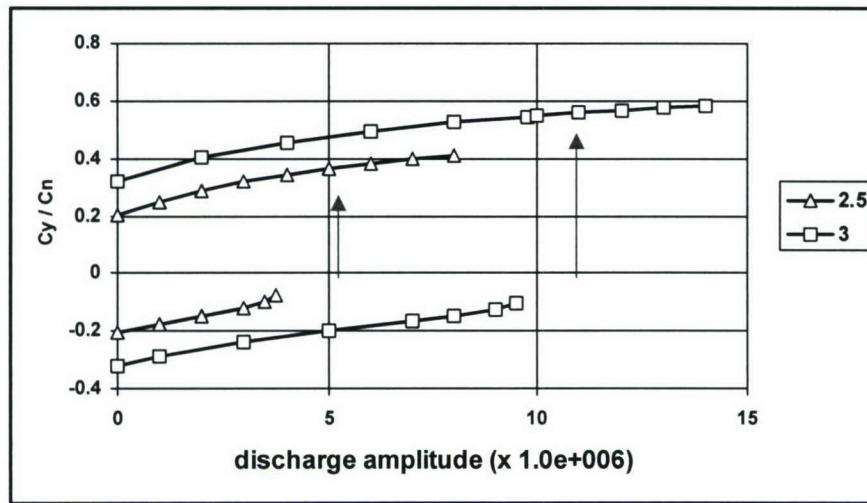
Figure 20 Normalized side force coefficient as a function of source intensity; the energy source is located on the cone side where the vortex is closer to the cone surface; line with triangles – $\alpha = 2.5$, line with squares – $\alpha = 3$.

The foregoing numerical results indicate that it is not feasible to achieve symmetric flow using an energy source located only on one side of the cone surface. At first glance, this contradicts experiment [P5], where a smooth variation of the vortex structure versus the discharge power was observed and the symmetric flow was achievable. However, in these experiments the energy source was located near the cone nosetip, and the flow patterns were examined far downstream from the discharge region, where there was no energy addition to the flow. This case can be treated using the spatial-temporal similarity; i.e., the streamwise evolution is similar to the temporal evolution with time $t = x/u$, where x is longitudinal coordinate and u is longitudinal velocity. Accordingly, the experimental data may be interpreted as data of an unsteady process. Initially (near the cone nose) there is asymmetric flow. Then the energy source forces the flow to evolve from the asymmetric state to nearly symmetric state. This occurs in the range of energy deposition. Then, the source is switched off and the nearly symmetric flow pattern relaxes to an asymmetric state with right or left asymmetry. The relaxation rate depends on the source power, its length and locus. At a certain combination of these parameters, the relaxation rate may be small. In this case, one can observe almost symmetric flow pattern over the cone of relatively short length. However, at sufficiently large distances from the source locus, the flow pattern will be asymmetric because the symmetric state is unstable.

In solving the conical Navier-Stokes equations, the iteration number of the convergence process may be treated as a time-like variable, if calculations are conducted with a constant time step for all grid cells. An example of such calculations is shown in Figure 21 for the case $\alpha = 3$. The energy source of $q_0 = 2 \times 10^7$ was turned on and then turned off as shown in the figure. The activation "time period" was chosen so that the side force was slightly positive by the end of forcing. In this case, the flow remains almost symmetric for a long "time period". Ultimately the flow evolves to the asymmetric state due to instability.
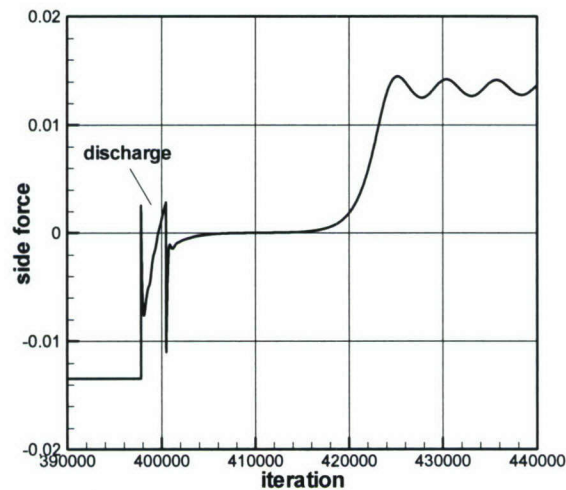
Figure 21 Evolution of the side force coefficient versus the iteration number; the energy source is active in the finite range indicated in the figure.

These features of CNS solutions indicate that it is important to perform adequate modeling of the transition process. Currently, we address this problem by solving the 3-D Navier-Stokes equations. Furthermore, the aforementioned numerical results are used for refinements of our lower-order models. The latter are needed to develop close-loop feedback systems for yaw control and tailless capability.

In summary, *the theoretical models and computational tools developed under this project make us well equipped to address the problem of plasma flow control for delta wings at high angles of attack.*

2.3 Experiments in ITAM

The theoretical feasibility studies of Section 2.1 initiated wind-tunnel experiments at ITAM under EOARD support (ISTC Project #2235). The experiments were performed on a slightly blunted cone at freestream speeds 10-24 m/s [P5,P8]. Two rows of electrodes were flush mounted along cone generators as shown in Figure 22. Spark discharges were ignited between the first pair of electrodes with the alternating voltage of frequency 400 Hz and voltage V~20kV. The total discharge power was varied in the range 20 – 100 W.

Without plasma discharges, the vortex structure has right asymmetry as shown by smoke visualization in Figure 23. With the spark discharge on the right side, the vortex structure has left asymmetry. The vortex asymmetry changes from right to left with gradual increasing of the discharge power. These experiments confirm our basic concept. More details of this experimental phase of the effort are given in [P5,P8]. *Therein a full description of our recent actual feasibility demonstration of the control concept is given in which an asymmetrical flow configuration was symmetrized by the surface discharge plasmas.* In this work, the important role of bluntness and laminar and turbulent separation cases was highlighted as well as the ability to symmetrize and initially unsymmetrical nose vortex pair due to delayed spark ignition on one

18

side of the cone. Subsequent ignition of this side symmetrized the unsymmetrical vortex configuration.

Experiments with variation of the surface discharge actuator power demonstrated that it is feasible to smooth variations of flow asymmetry and pressure distribution. This is of critical importance for stall-spin departure control.
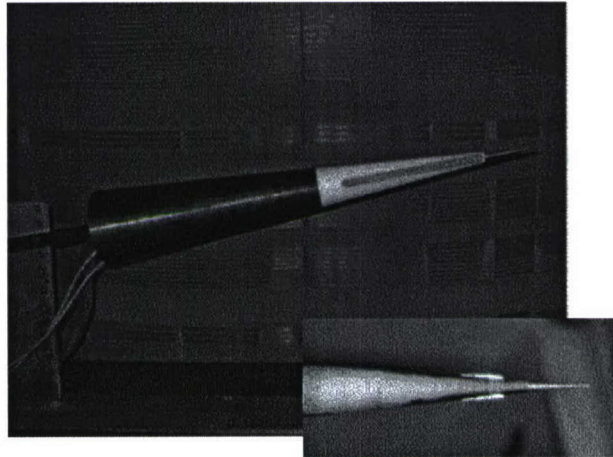
Figure 22 Blunt cone model with spark discharges.
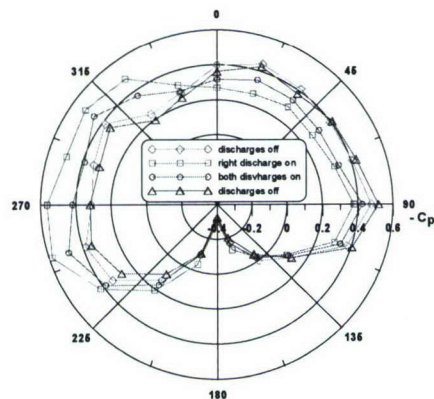
Distribution of pressure coefficient
U = 10 m/s, AOA = 22.5 deg.

No discharge   Right discharge is on   Right and left discharges are on
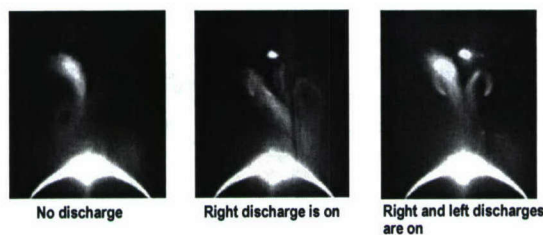
Figure 23 Demonstration of vortex flow control using spark discharges on a slender cone.

2.4 Plasma discharge modeling

Our modeling of the surface barrier discharge (SBD) was started under the ISTC project 2235. In FY 2002-2004, physical and mathematical models of SBD relevant to flow control applications have been formulated. The SBD configuration and its equivalent electrical scheme are shown in Figure Figure 24. The first electrode is a thin metal strip flush-mounted on the cone surface energy input line. The second electrode is mounted under the first one. The electrodes are separated from each other by a dielectric layer of thickness d and the relative permittivity ε. The discharge evolves along the first electrode edge, if the electrodes are supplied by an alternating voltage of appropriate frequency and the voltage amplitude is high enough for air breakdown. In atmospheric air, this discharge burns stably in the form of a thin line along the electrode edge for alternating voltage frequency f=1-100 kHz and voltage amplitude greater than few kilovolts [29, 30].

The surface barrier discharge is a set of short, temporally repetitive streamers propagating perpendicular to the electrode edge. To 10 ns accuracy, all streamers start simultaneously in each streamer set [31]. These sets are separated from each other by the time interval $\Delta\tau \approx 30$ µs for an external voltage frequency f=1kHz (Figure 25).
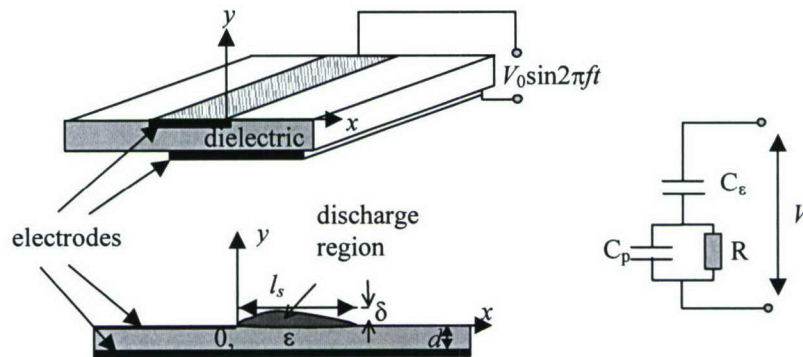
Figure 24 Electrode layout for surface barrier discharge and its equivalent electrical scheme.
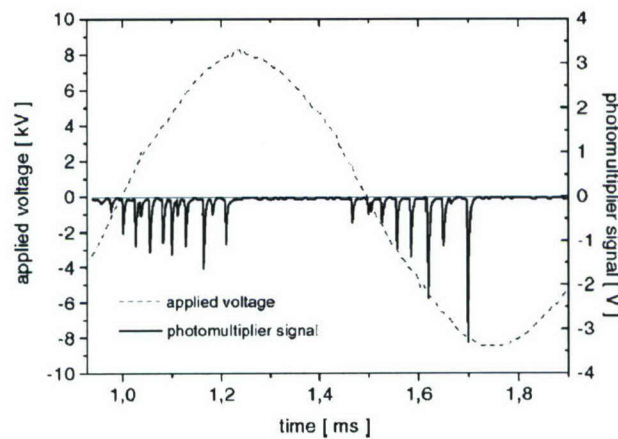
Figure 25 Current pulses (spikes) associated with SBD for alternating voltage (dashed curve) of frequency f=1kHz [31].

For $f \ll 1/\Delta\tau$, the streamer distribution along the electrode edge is chaotic with no anchoring to any fixed points. Accordingly, the dust visualization of SBD [32] (Figure 26) shows that the discharge region uniformly covers a strip along the electrode edge. The strip width, l_s, depends on the electrode polarity, voltage amplitude and ε (Figure 27).
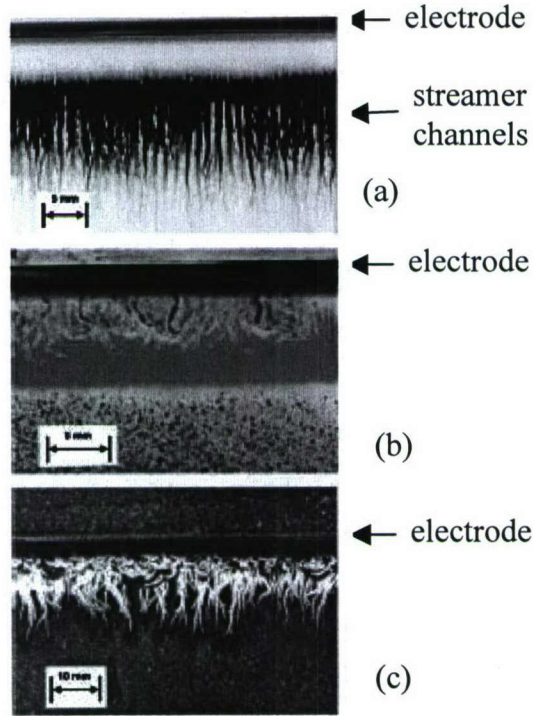
Figure 26 Dust visualization of SBD [29]: (a) - positive voltage pulse of 20 kV; (b) – negative voltage pulse of 20 kV; (c) – alternating voltage of 10 kV.
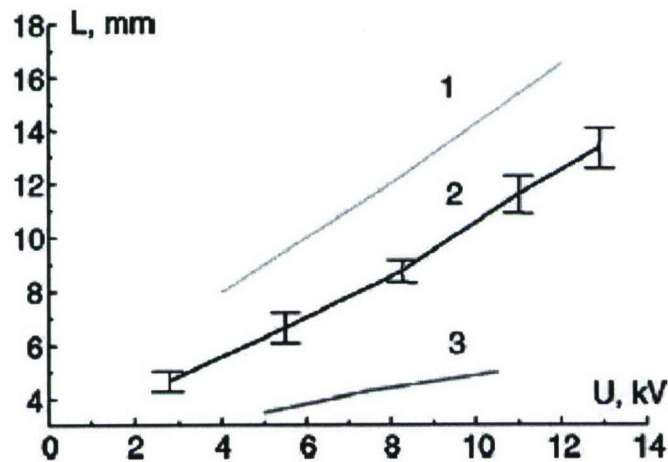
Figure 27 SBD average streamer length l_s as a function of the applied voltage (ε=5, d=2mm) for positive (1), negative (3) and alternating (2) surface electrode polarity [29].

The problem of surface discharge evolution in the near wall region was formulated in a 2-D approximation using aerodynamic models for the boundary layer and previously developed kinetic models for SBD [30]. We focused on the case of maximum average power deposition, when only one current pulse occurs on each half of the applied voltage period (this corresponds to the applied voltage frequency $f \sim$ 100-300 kHz). The following phases of SBD burning were identified:

- Phase A of $\tau_{imp} \approx$ 30-50 ns is associated with discharge formation and development. This phase is characterized by an electric field of breakdown level.

- Phase B of $\Delta\tau \sim 1/(2f) \approx$ 2-5 μs is relevant to intervals between the neighboring current pulses of opposite polarity.

Analysis of the SBD kinetic processes show:

- For modeling of Phase A, electron impact ionization, dissociative attachment and, possibly, electron detachment need to simulated.

- For modeling of Phase B, electron attachment and detachment as well as the ion-ion recombination processes should be included.

Since Phase A is much shorter than Phase B, the former can be modeled separately. Namely, Phase A can be treated as the SBD development corresponding to an electrical current pulse flowing through the gas due to electron and ion drift and diffusion. The electron detachment from negative ions and recombination processes can be neglected. In this approximation, the problem was formulated and solved numerically using Particle-in-Cell (PIC) method for the transport equations and the improved Gauss-Seidel (upper relaxation) method for the Poisson equation governing the electric potential.

First-cut calculations showed that the aforementioned model is not correct. The initially volumetric distribution of electrons are convected by the electric field to the dielectric surface without sufficient production, so that the discharge ceases before the electron concentration reaches a value sufficient for air glowing. To improve the model, the air ionization by UV photons emitted by discharge region should be taken into account. Photo-ionization is a key mechanism for barrier discharge development, because it may create new electron-ion pairs in the region of high electric field that, in turn, gives rise to new electron avalanches.

In FY 2005, the modified problem, which includes the photo-ionization effect, was solved numerically. These solutions represent the streamer phase of less than 10-20 ns duration. Calculations were carried out for different polarity of applied constant voltage $V = \pm$ 7kV. The upper electrode occupies the region $x < 0$, $0.1 > y > 0$. Figure 28 and Figure 29 show the longitudinal component of volumetric force density and the time-averaged power deposition for a negative electrode potential ($V = -7$kV). Similar data for the positive electrode potential ($V = 7$kV) are shown in Figure 30 and Figure 31. The spatial distributions of momentum and energy sources are quite different. For negative potential, the momentum and energy sources are attached to the surface. For a positive potential, these sources peak in the volume located at a distance $\sim$ 0.1mm from the dielectric surface.

The absolute values of energy and momentum sources are greater for a positive electrode potential. Since the force acting on the carrier gas is directed from positive to negative electrode,

the momentum transfer to the gas produced by positive ions is greater than that produced by the electrons. The absolute value of the force due to this momentum transfer coincides in order of magnitude with the estimates based on experimental observations.

The foregoing results indicate that our physical and numerical models capture the streamer phase of SBD evolution. This provides a good starting point to address the relaxation phase B and treat the whole SBD cycle produced by an alternating applied voltage.
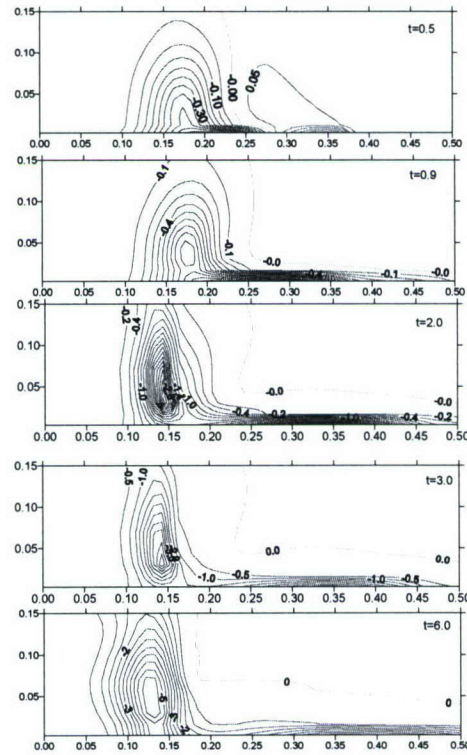
Figure 28 Contours of time averaged x-component of volumetric force density (in units of MDyn/cm^3) for negative electrode polarity (V = -7kV); time t is in units of 1.78 ns.
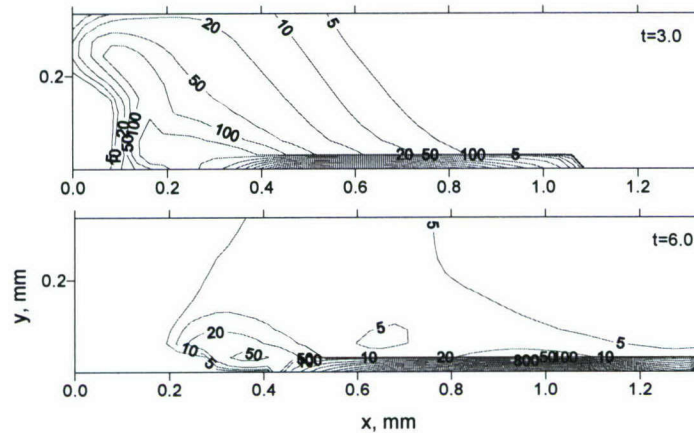
Figure 29 Contours of time averaged power deposition W (in units of kW/cm^3) for negative electrode polarity (V = -7kV); time t is in units of 1.78 ns.

23
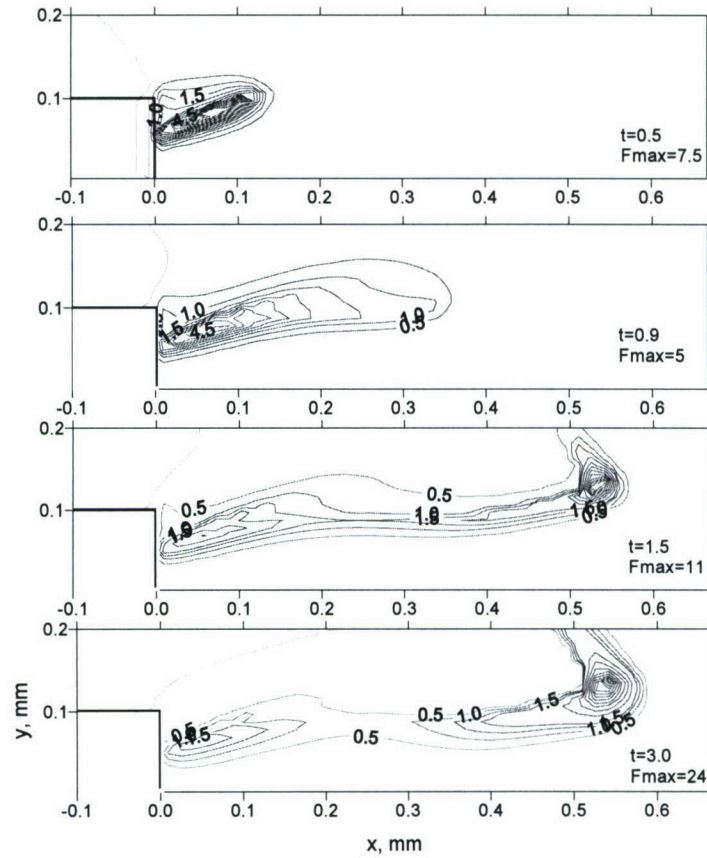
Figure 30 Contours of time averaged *x*-component of volumetric force density (in units of MDyn/cm^3) for positive electrode polarity (V = +7kV); time *t* is in units of 1.78 ns.
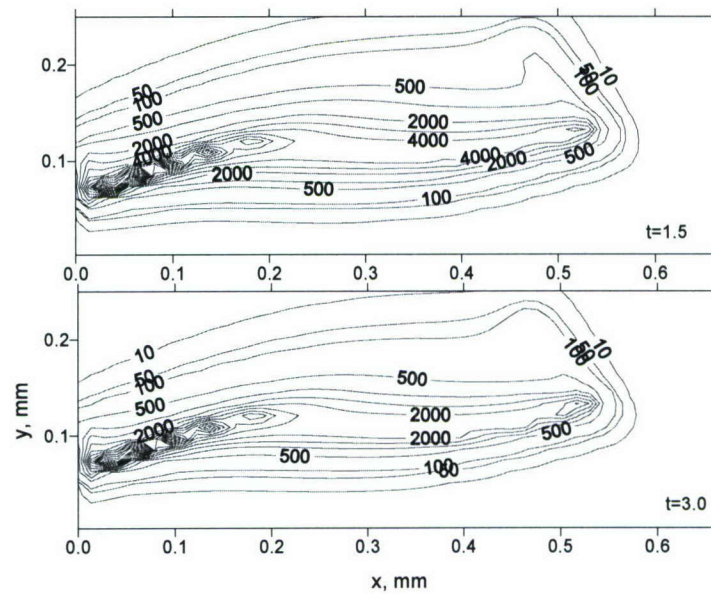
Figure 31 Contours of time averaged power deposition *W* (in units of kW/cm^3) for positive electrode polarity (V = +7kV); time *t* is in units of 1.78 ns.

24

TELEDYNE
SCIENTIFIC COMPANY
A Teledyne Technologies Company

3. Summary and Impact of Effort

The first phase of this program clearly confirmed that nose tip-vortex symmetry breaking strongly depends on the boundary-layer separation locus. Results of this research provided strong evidence supporting our original conjecture that this locus can be effectively controlled by a surface discharge located upstream from the separation line. From the lower-order theoretical models, it was shown that with strategically located discharges of relatively small power (less than 1 kW) it is feasible to shift the separation line toward the windward surface and stabilize the symmetric vortex configuration as well as make it robust to symmetry-breaking small perturbations. Such power levels can be easily accommodated on aircraft. Under complementary EOARD support, the Institute of Theoretical and Applied Mechanics (ITAM, Novosibirsk) performed a first series of wind-tunnel experiments validating the theory and even provided a working spark discharge arrangement that avoids symmetry-breaking on a conical nose tip, typical of actual aircraft shapes.

In the second phase, the effort has been focused on development of more comprehensive computational tools, which could provide data for validation and calibration of our lower-order theoretical models. By examining available numerical methods, which have been used for modeling of the vortex flow over a cone at high angles of attack, we concluded that methods based on the Conical Navier-Stokes (CNS) equations fit our needs. The CNS equations are an approximate form of the 3-D Navier-Stokes equation. They differ from the full equations by the assumption of constant properties in the radial direction. Nevertheless, the conical solutions reproduce symmetric and asymmetric vortex configurations, which are similar to those observed in experiments. As contrasted to our earlier lower-order models, in which the separation points were fixed à priori, the CNS method captures the interaction between viscous boundary layer and inviscid outer flow and predicts separation lines.

The Conical Navier-Stokes (CNS) solver was developed and applied to simulate vortex structures over a cone at high angles of attack for laminar and turbulent flows. Numerical solutions satisfactorily predict characteristics of symmetric and asymmetric vortex structures for laminar and turbulent flows observed in the subsonic wind-tunnel experiments. The CNS solver was used for modeling of the spark-discharge effect on vortex asymmetry past a sharp cone at high angles of attack. To simulate local heating induced by the discharge, a source term was added to the energy equation. The CNS predictions qualitatively agree with the experimental observations. Namely, the heat source causes early separation and reduces the vortex flow asymmetry. With two symmetric heat sources located on opposite sides of the cone cross-section it is feasible to restore the symmetric flow pattern and eliminate the side force. Numerical studies showed that the side force reveals a hysteretic behavior versus the source intensity. The side force control law may reveal non-monotonic features depending on the angle of attack and the heat source intensity.

The major gap in plasma flow control technology is the lack of self-consistent theoretical models and robust computational tools providing adequate simulation of heat and momentum sources induced by surface plasma discharges. First steps in solving this problem were made for the surface barrier discharge (SBD). The developed physical and numerical models capture the streamer phase of SBD evolution. This provides a good starting point to address the relaxation phase and treat the whole SBD cycle produced by an alternating applied voltage.

The findings summarized herein encourage us to continue the theoretical and computational effort that will interact with wind tunnel testing of ITAM. With our refined theoretical and CFD tools, we are well positioned to investigate effects of external forcing produced by surface plasma dischargers and address the problem of plasma stall spin departure control and other aerodynamic augmentation such as separation, transition and vortex control and virtual morphing of high altitude, long endurance flight vehicles.

References

1. Skow, A.M., and Peake, D.J., "AGARD Lecture Series No. 121, "High Angle of Attack Aerodynamics," AGARD-LS-121, pp. 10-1–10-22, March 1982.

2. AGARD Lecture Series No. 121, "High Angle of Attack Aerodynamics," AGARD-LS-121, March 1982.

3. Hunt, B.L., "Asymmetric Vortex Forces and Wakes on Slender Bodies," AIAA Paper No. 82-1336, 1982.

4. Ericsson, L.E., and Reding, J.P., "Aerodynamic Effects of Asymmetric Vortex Shedding from Slender Bodies," AIAA Paper No. 85-1797, 1985.

5. Keener, E.R., Chapman, G.T., Cohen, L., and Telegani, J., "Side Forces on Forebodies at High Angles of Attack and Mach Numbers of 0.1 to 0.7: Two Tangent Ogive, Paraboloid and Cone," NASA TM X-3438, 1977.

6. Keener, E.R., "Oil Flow Separation Patterns on an Ogive Forebody," *AIAA J.*, **21**, No. 4, pp. 550–556, 1983.

7. Lamont, P.J., and Hunt, B.L., "Pressure and Force Distributions on a Sharp-Nosed Circular Cylinder at Large Angles of Inclination to an Uniform Subsonic Stream," *J. Fluid Mech.*, **76**, No. 3, pp. 519–529, 1976.

8. Dexter, P.C., "A Study of Asymmetric Flow over Slender Bodies at High Angles of Attack in Low Turbulence Inviroment," AIAA Paper No. 84-0505, 1984.

9. Lamont, P.J., "Pressure around an Inclined Ogive Cylinder with Laminar, Transitional, or Turbulent Separation," *AIAA J.*, **20**, No. 11, pp. 1492 - 1499, 1982.

10. Lamont, P.J., "The Effect of Reynolds Number on Normal and Side Forces on Ogive Cylinder at High Incidence," AIAA Paper No. 85-1799, 1985.

11. Champigny, P., "Influence du nombre de Reynolds sur les caracteristiques aerodynamics d'une configuration ogive-cylindre a grand incidence," *Recherche Aerospatiale*, No. 6, pp. 417 - 425, 1984.

12. Moskovitz, C.A., Hall, R.M., and De Jarnette, F.R., "Effects on of Nose Bluntness, Roughness and Surface Perturbations on the Asymmetric Flow past Slender Bodies at Large Angles of Attack," AIAA Paper No. 89-2236, 1989.

13. Ziliac, G.G., Degani, D., and Tobak, M., "Asymmetric Vortices on a Slender Body of Revolution," *AIAA J.*, **29**, No. 5, pp. 667–675, 1991.

14. Lowson, M.V., and Ponton, A.J.C., "Symmetric Breaking in Vortex Flows on Conical Bodies," *AIAA J.*, **30**, No. 6, pp. 1576 - 1583, 1992.

15. Tobak, M., and Peake, D.J., "Topology of Three-Dimensional Separated Flows," Annual Review of Fluid Mechanics **14,** pp. 61 - 85, 1982.

16. Fiddes, S.P., "Separated Flow about Cones at Incidence–Theory and Experiments," Studies of Vortex Dominated Flows, Springer Verlag, NY, pp. 185–310, 1987.

17. Hartwich, P., Hall, R., and Hemsch, M., "Navier-Stokes Computations of Vortex Asymmetries Controlled by Small Surface Imperfections," AIAA Paper No. 90-0385, 1990.

18. Degani, D., "Numerical Investigation of the Origin of Vortex Asymmetry," AIAA Paper No. 90-0593, 1990.

19. Siclari, M.J., "Asymmetric Separated Flows at Supersonic Speeds," AIAA Paper No. 90-0595, 1990.

20. Poll, D.I.A.,"Some Effects of Boundary Layer Transition on Slender Axisymmetric Bodies at Incidence at Incompressible Flow," AGARD Symposium on Missile Aerodynamics, Tronheim, Norway, Paper 13, 1982.

21. Champigny, P.G., "Stability of Side Forces on Bodies at High Angles of Attack," AIAA 4th Applied Aerodynamic Conference, pp. 72–78, 1986.

22. Siclari, M.J., "Asymmetric Separated Flows at Supersonic Speeds," *AIAA J.,* **30,** No. 1, 1992.

23. Morrison, J.H., "A compressible Navier-Stokes Solver with Two-Equation and Reynolds Stress Turbulence Closure Models," NASA CR-4440, May 1992.

24. Abid, R., Morrison, J.H., Gatski, T.B., and Speziale, C.G., "Prediction of Aerodynamic Flows with a New Explicit Algebraic Stress Models," *AIAA J.*, **34,** No. 12, 1996.

25. Zhang, H.S., So, R.M.C., Gatski, T.B., and Speziale, C.G., "A New-Wall Second-Order Closure for Compressible Turbulent Flows," *Near-Wall Turbulent Flows,* Eds. R.M.C. So, C.G. Speziale, and B.E. Launder, Elsevier Science Publishers B.V., 1993.

26. Zhang, H.S., So, R.M.C., Speziale, C.G. and Lai, Y., *AIAA J.*, **31,** No. 1, 1993.

27. Speziale, C.G., Abid, R. and Anderson, E., "A Critical Evaluation of Two-Equation Model for Near Wall Turbulence," AIAA Paper No. 90-1481, 1990.

28. Peake, D.J., Owen, F.K. and Johnson, D.A., "Control of Forebody Vortex Orientation to Alleviate Side Forces," AIAA Paper No. 80-0183, 1980.

29. Samoilovich V., Gibalov V., and Kozlov K., *Physical Chemistry of the Barrier Discharge, 2nd edn.*, Dusseldorf: DVS, 1997.

30. Aleksandrov N.L., Bazelyan E.M., and Konchakov A.M., *Physika Plazmy*, **27,** 2001, p. 928.

31. Gibalov V.I., and Pietsch G.J., *J. Phys. D: Appl. Phys.*, **33,** 2000, pp. 2618-2636.

32. Post, M., and Corke, T., "Separation Control Using Plasma Actuators - Stationary and Oscillating Airfoils," AIAA Paper No. 2004-0841, 2004.

Publications

P1. Shalaev, V., Fedorov, A., Malmuth, N., Zharov, V., and Shalaev, I., "Plasma Control of Forebody Nose Vortex Symmetry breaking," AIAA Paper No. 2003-0034.

P2. Fedorov A., Shiplyuk, A., Maslov, A., Burov, E., and Malmuth, N., "Stabilization of High Speed Boundary Layer Using a Porous Coating," AIAA Paper No. 2003-1270, Reno NV, Jan. 6-9, 2003.

P3. Fedorov, A., Shiplyuk, A., Maslov, A., Burov, E., and Malmuth, N., "Stabilization of a Hypersonic Boundary Layer Using an Ultrasonically Absorptive Coating," *J. of Fluid Mechanics*, **479**, 2003, pp. 99-124.

P4. Shalaev, V., Fedorov, A., Malmuth, N., and Shalaev, I., "Mechanism on Forebody Nose Vortex Symmetry Breaking Relevant to Plasma Flow Control," AIAA Paper No. 2004-842, Reno Nevada, Jan. 5-9, 2004.

P5. Maslov, A., Zanin, B., Sidorenko, A., Fomichev, V., Pavlov, A., Postnikov, B., and Malmuth, N., "Plasma Control of Separated Flow Asymmetry on a Cone at High Angle of Attack," AIAA Paper No. 2004-0843, 42nd AIAA Aerospace Sciences Meeting and Exhibit, Reno, NV, January 4-7, 2004.

P6. Malmuth, N.D., "Theoretical Aerodynamics in Today's Real World, Opportunities and Challenges," Julian D. Cole Lecture. AIAA Paper 2005-5059, 2005.

P7. Malmuth, N., and Fedorov, A., "The Shock Layer Model for a Jet in a Hypersonic Cross Flow," AIAA Paper No.2005-893, 43rd AIAA Aerospace Sciences Meeting and Exhibit, 10-13 Jan. 2005, Reno Nevada.

P8. Maslov A.A. et al, "Two-Channel Spark Discharge for Flow Control on a Body of Revolution," AIAA Paper No. 2005-040, 2005.

P9. Maslov, A., Shiplyuk, A., Sidorenko, A., Polivanov , P., Fedorov, A., Kozlov, V., and Malmuth, N., ":Hypersonic Laminar Flow Control Using a Porous Coating of Random Microstructure," AIAA Paper 2006-1112, Reno NV.

P10. Zakharov, S.B., Fedorov, A.V., and Malmuth, N.D., "Modeling of Forebody Nose Vortex Symmetry Breaking Using Conical Navier-Stokes Solutions," AIAA Paper 2006-1257, Reno NV.

P11. Zhakharov, S.B., Fedorov, A.V., and Malmuth, N.D., "Modeling of Forebody Nose Symmetry Breaking Using Conical Navier-Stokes Solutions," AIAA Paper No. 2006-1257, 9-12 Jan. 2006, Reno NV.

P12. Malmuth, N.D., Zhakharov, S.B., and Fedorov, A.V., "Conical Navier-Stokes Modeling of Forebody Vortex Symmetry Plasma Control," AIAA Paper No. 2007-948, 9-12 Jan. 2007, Reno NV.

P13. Malmuth, N.D., Zakharov, S.B., and Fedorov, A.V., "Conical Navier-Stokes Modeling of Forebody Vortex Symmetry Plasma Control," AIAA Paper No.2007-219, 45th AIAA Aerospace Sciences Meeting and Exhibit, 8-11 Jan. 2007, Reno NV.

P14. Fedorov, A. V., Malmuth, N. D., and Soudakov1 V. G., "Supersonic Scattering of a Wing-Induced Incident Shock by a Slender Body of Revolution," *J. of Fluid Mechanics*, accepted for publication in 2007.